Investigation of nuclear forces in d + p elastic and p + d break-up reactions at intermediate energies

Mardanpour-Mollalar, Hossein

6. Analysis of the $\vec{p}+d$ break-up reaction

In this chapter, the analysis of the $\vec{p}+d \rightarrow p+p+n$ reaction is described. The experiment exploits BINA and uses a polarized proton beam with an energy of $E^p_{lab} = 190$ MeV impinging on a liquid deuterium target.

The main objective of this chapter is to present the procedure of obtaining the cross sections and vector-analyzing powers. In the following, the kinematics of the $\vec{p}+d$ break-up reaction are introduced as a function of the coordinates of the detected particles. Then, the necessary steps such as: the energy calibration of the E-detectors, and the study of the background structure are explained in details. Finally, the results for the cross section and analyzing power are shown for one of many configurations.

6.1 Break-up kinematics and the S-curve

The kinematics of the break-up reaction are defined using the spherical coordinates of the observed particles. As it was discussed in Chap. 2, for the $\vec{p}+d \rightarrow p+p+n$ reaction, the total number of parameters are 9, $(\theta_1, \theta_2, \theta_3,\ \phi_1, \phi_2, \phi_3,\ E_1, E_2, E_3)$, and there are 4 equations that come from the energy and the momentum conservation laws. Therefore, by measuring 5 of these parameters, all other observables can be obtained analytically. Conventionally, in the $\vec{p}+d$ break-up reaction, the kinematics are determined by using the scattering angles of the two protons, $(\theta_1, \theta_2, \phi_{12} = \phi_1 - \phi_2)$, and the correlation between their energies presented by the kinematical curve which is called the S-curve. For

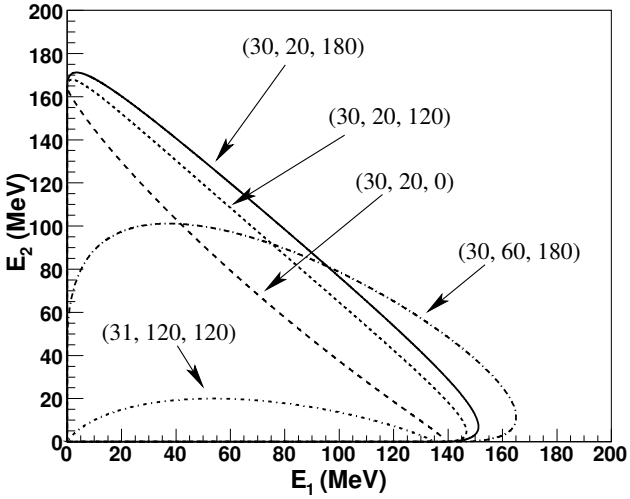

Figure 6.1: The energy correlation between two protons in coincidence is shown as the S-curves for several kinematical configurations. The kinematics are defined by $(\theta_1, \theta_2, \phi_{12} = \phi_1 - \phi_2)$, the polar scattering angles of the first and the second proton, respectively, and the relative azimuthal angle. Angles are given in degrees.

example, Fig. 6.1 shows the S-curve for several kinematical configurations. In general, the maximum energy of particles that scatter to forward angles is larger than the maximum energy of those that scatter to the backward angles. In this figure, the line labeled as $(31^\circ, 120^\circ, 120^\circ)$ shows a coincidence of two protons of which one scatters to $\theta = 31^\circ$ while the second proton scatters to $\theta = 120^\circ$, and the azimuthal opening angle, ϕ_{12}, between them is 120°. The maximum energy of the backward scattering proton is lower than 25 MeV. For some of the kinematics where one of the protons scatters to angles larger than 140°, the energy of the proton is lower than the detection threshold of the ball detectors of BINA. Therefore, these configurations are not covered by BINA. This energy threshold will be discussed in the following sections.

6.2 Energy calibration of the E detectors for the break-up channel

The energy calibration of the scintillators is the first step in the analysis of the data. The energy calibration of BINA for the break-up events is divided into two parts:

1. The calibration of the forward-wall E scintillators,
2. The calibration of the backward-ball scintillators.

The forward E scintillators can be calibrated using precise measurements of the scattering angles using the MWPC. These precise scattering angles are used to distinguish between different kinematical configurations. The ball scintillators are used to determine the scattering angles of the backward-scattered particles. These scattering angles are not as precise as the MWPC measurement and the kinematics are, thus, defined with lower resolutions.

6.2.1 Energy calibration of the forward E scintillators

The energy calibration of the forward E scintillators are performed using the response of PMTs at both ends of each scintillator. By using the $\sqrt{L_{chan} \times R_{chan}}$ as a measure for the energy, we can partly compensate for the light attenuation, as discussed in Chap. 5, in the scintillators, and have an almost linear relation between detected signal and the deposited energy in MeV at all positions in the scintillators. To perform the energy calibration of the break-up channel, the kinematical correlation between the energies of the outgoing protons can be exploited. We choose a coplanar kinematical configuration, $(\theta_1, \theta_2, \phi_{12}) = (28^\circ, 28^\circ, 180^\circ)$, as the starting point to calibrate the forward E scintillators. This part of the phase space has a high cross section, which provides enough statistics to perform a precise calibration. In addition, this configuration covers all the scintillators in the forward part of BINA. In this configuration, the two protons are coplanar and scatter to two opposite scintillators on the top and the bottom of the forward-wall. The calibration of the E detectors is performed in groups of two scintillators. Figure 6.2 shows the deposited energy (chan no.) for protons from the break-up channel in scintillator 1 (Y-axis) versus scintillator 10 (X-axis).

The energy of the protons at the scintillator is less than the energy of the protons at the target due to the energy losses caused by materials between the target and the

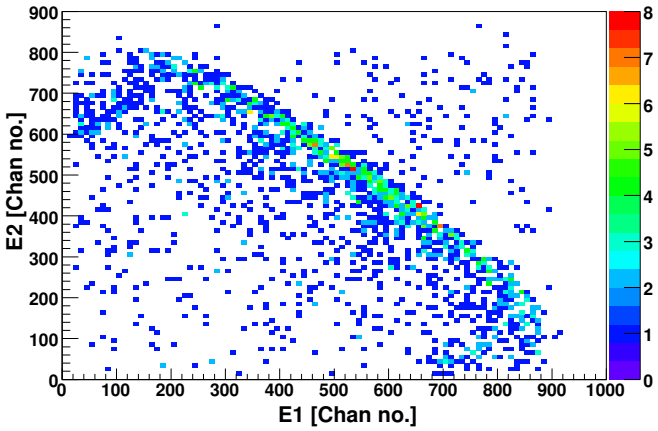

Figure 6.2: The correlation between signals of two scintillators for the coplanar kinematical configuration, $(\theta_1, \theta_2, \phi_{12}) = (28°, 28°, 180°)$. The deposited energy of protons in scintillator 1 (Y-axis) is plotted versus that in scintillator 10 (X-axis) in channel unit. These data are used for the energy calibration of these two E scintillators.

scintillator. So, in this stage we cannot use the S-curve to calibrate the scintillators. For this purpose, we use the energy response from a GEANT-3 simulation. In this simulation, all the components, such as the target holder, the opening flange of BINA, the MWPC, ΔE scintillators, air medium, cover of the scintillators, and E scintillators are implemented and the energy losses have been determined. The left panel in Fig. 6.3 shows the deposited

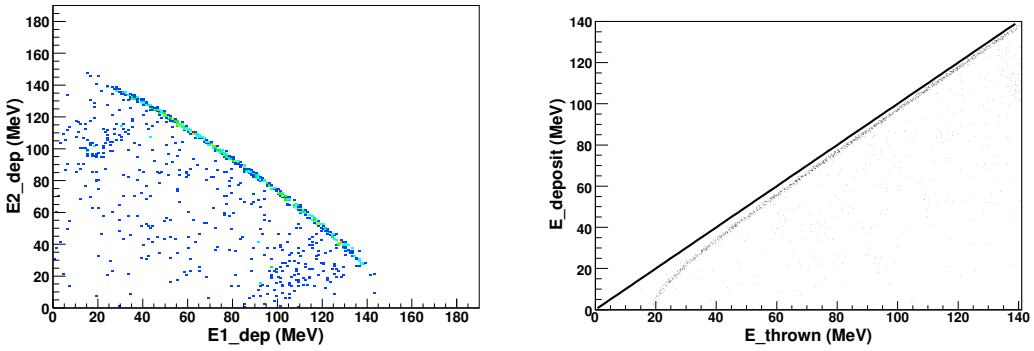

Figure 6.3: The response of the E scintillator according to the GEANT-3 simulation for the break-up reaction. The left panel shows the correlation between the deposited energy of two protons for kinematical configuration, $(\theta_1, \theta_2, \phi_{12}) = (28°, 28°, 180°)$. The right panel shows the correlation between the deposited energy of a proton and its thrown energy (generated energy) in the energy range from 0-140 MeV. A diagonal solid line is added to show the deviation from the linear response for different energies. The simulated data in this graph are used as the reference for the energy calibration of the forward E scintillators of BINA.

energies of two protons in the GEANT-3 simulation. The channel numbers in Fig. 6.2 are multiplied by a linear calibration factor to fit to the graph from Fig. 6.3. After this

calibration, we correct the deposited energy (MeV) by the energy losses to obtain the energy at the target position. In the right panel of Fig. 6.3, the simulated energy of the protons at the target, E_{thrown}, is plotted versus the deposited energy at the scintillator, $E_{deposit}$, obtained from the GEANT-3 simulation. A diagonal solid line is added to the graph to show the deviation from the linear response for different thrown energies. It can be seen that the losses at small energies are larger than at high energies, as one would expect.

The calibration procedure, described above, is applied to all the scintillators. Figure 6.4 shows the calibrated energy of two protons for $(\theta_1, \theta_2, \phi_{12}) = (28°, 28°, 180°)$ where data from all the scintillators are added. The S-curve for this configuration is plotted as a solid line to show the quality of the energy calibration for the forward E scintillators. Protons with an energy of less than 25 MeV at the target position are rejected.

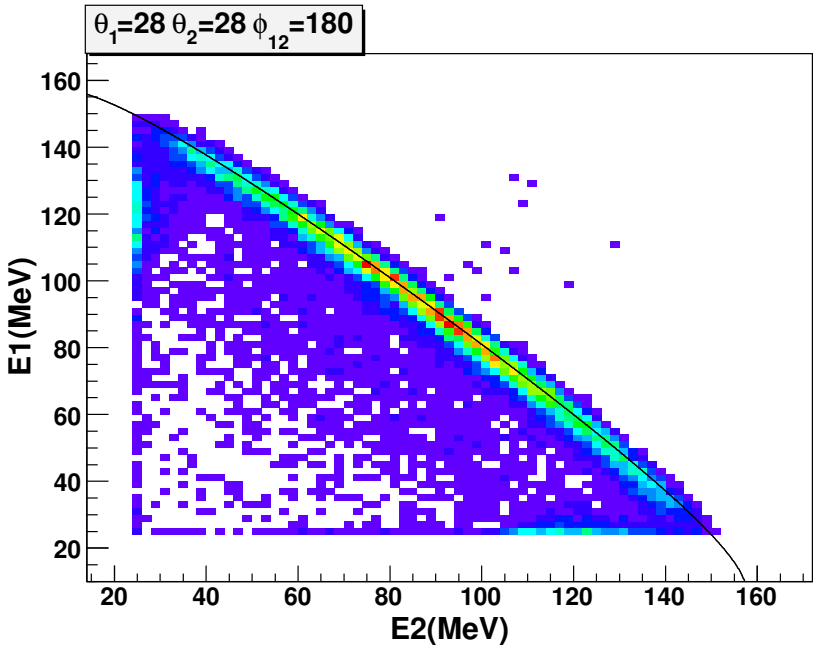

Figure 6.4: The correlation between the calibrated energy of the two outgoing protons in the break-up process is shown for the coplanar configuration, $(\theta_1, \theta_2, \phi_{12}) = (28°, 28°, 180°)$. The relativistic S-curve which is calculated from energy and momentum conservation is added to the picture, as a solid line. Protons with an energy of less than 25 MeV at the target position are rejected.

In the break-up reaction, the maximum energy of protons in the forward part can be very close to the energy of a proton originating from elastic scattering. As it was discussed in Chap. 5, protons with an energy $E_p > 140$ MeV punch through the forward scintillators. A fraction of this energy is deposited while the rest escapes from the system. These particles deposit an average energy between 90-140 MeV in the scintillators, depending on their initial energy at the reaction point. Figure 6.5 illustrates the regions for which the protons punch through the scintillators.

The energy losses due to the punch-through effect can be calculated and corrected for

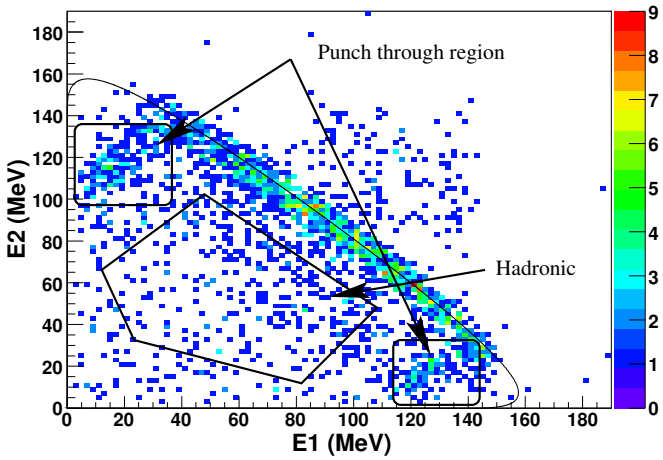

Figure 6.5: The calibrated energy correlation between two protons is shown for the same kinematics as in Fig. 6.4. The punch-through regions are indicated at both ends of the S-curve. In these regions, the energy of one of the protons is larger than 140 MeV and this proton punches through the scintillators. In the punch-through regions, the deposited energy of the second proton is less than 20 MeV. The hadronic events are, also, indicated in the picture. These events are true break-up events, but they deposit less energy due to hadronic interactions.

protons by exploiting the kinematical correlation between the two protons of the break-up reaction (solid lines in Fig. 6.5). In the present data analysis, we decided to consider only the part of the S-curve for which both protons stop in the scintillators. Therefore, protons with a thrown energy of less than 25 MeV were rejected. Other experiments which were carried out with BINA at lower energies: $\vec{p}+d$ @ $E_p = 130$ MeV, $\vec{d}+d$ @ $E_d = 130$ MeV, and $\vec{d}+p$ @ $E_d = 100$ MeV, do not suffer from this problem.

6.2.2 Energy calibration of the backward ball

The energy calibration of the backward part of BINA is more difficult than the calibration for the forward wall, since the backward-scattered particles are detected by the ball scintillators which have a relatively low angular resolution, $\Delta\theta = \Delta\phi = \pm 10^\circ$. Consequently, break-up events within this interval do not have a clear correlation between the energies of the final-state protons. As it was mentioned in Chap. 5, we divided the ball scintillators into three regions:

1. $40^\circ < \theta < 80^\circ$, this region has a large number of deuterons from the elastic channel. Therefore, we can use the ball calibration performed with deuterons multiplied by a constant scaling factor which gives the energy calibration for protons (see Fig. 6.6).

2. $80^\circ < \theta < 110^\circ$, this region can be calibrated using protons. However, because of the shadow of the target holder, two groups of particles are detected in these scintillators. The first group consists of protons that passed through the target holder material and lose part of their energy, and the second group comes from the protons that did

not hit the target holder. Due to lack of time, we decided not to use this angular range for the current phase of the data analysis.

3. $\theta > 110°$, for this region we can use the calibration parameters of protons from the elastic channel. (see Fig. 6.7).

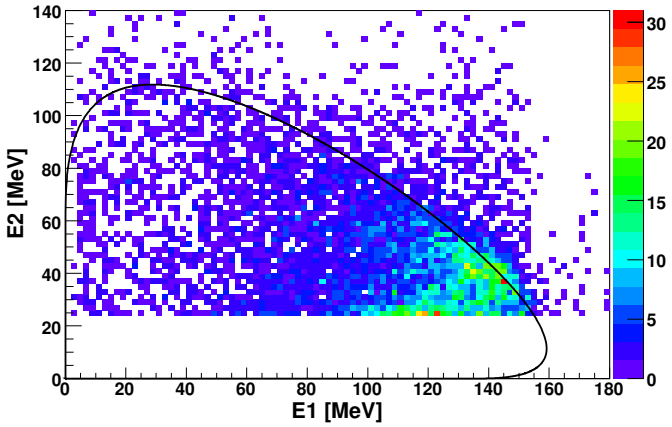

Figure 6.6: The energy correlation between protons registered in the forward part, (E_1), with protons in the first region of the ball (E_2), $(\theta_1, \theta_2, \phi_{12}) = (30° \pm 1°, 53° \pm 10°, 160° \pm 10°)$. The data are dominated by the background protons from the elastic channel which punch through the forward part of detector. These events appear around $E_1 = 100$ MeV.

Figure 6.7 shows the correlation between the energy of protons registered in the forward wall, with that of protons in the backward hemisphere of the ball (region 3) for the configuration, $(\theta_1, \theta_2, \phi_{12}) = (30° \pm 1°, 110° \pm 10°, 30° \pm 10°)$. Since, the angular resolution of the ball detectors is around $\Delta\theta = \Delta\phi = 10°$ (size of one detector), which is much larger than an angular bin obtained from the forward wall, the corresponding S-curve will be much broader than the one seen in Fig. 6.4. Consequently, a comparison between a well-defined S-curve and data is more difficult. Also, for these ball-wall configurations, it is possible that protons punch through the detector, for which a detailed analysis is necessary. Such events were registered and identified in the experiment, but their analysis would be more elaborate and requires Monte-Carlo simulations of the acceptance of the detectors.

6.3 Background analysis in the spectrum of the break-up reaction

In this section, the structure of background for the break-up reaction is discussed. In our data analysis, an event is labeled as a break-up event if two successful tracks are reconstructed in the forward part of BINA. The energies of protons which stem from a break-up reaction have a distinct correlation, represented by the kinematical S-curve. Therefore, events which do not correlate according to the expected S dependence will be

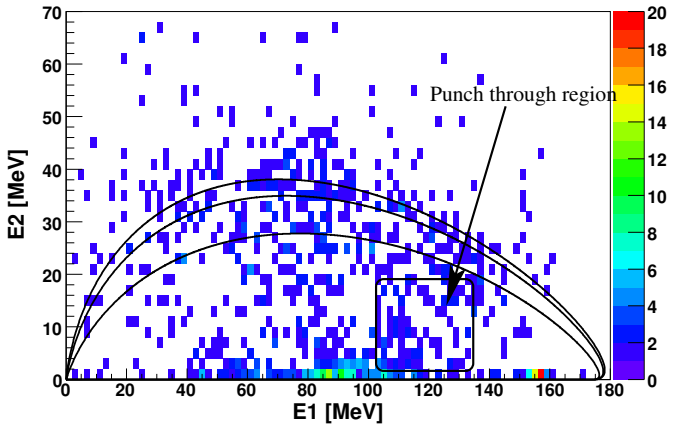

Figure 6.7: The energy correlation between protons registered in the forward wall of BINA (E_1), with protons in the third region of the ball (E_2) for $(\theta_1, \theta_2, \phi_{12}) = (30° \pm 1°, 110° \pm 10°, 30° \pm 10°)$. The maximum energy of the backward-scattered particles is ∼40 MeV, and the maximum detected energy of the forward-scattered particle does not exceed the punch-through limit of 140 MeV. The events which punch through the detector can be observed at lower values of S.

rejected. With this condition, a small percentage of good events which undergo a hadronic interaction are lost. This has been corrected for.

The total cross section of the elastic channel is comparable with that of the break-up reaction. However, since the phase space of the elastic channel is much more confined than the break-up reaction, the count rate of elastic-scattering events in the forward part is much higher than that of the break-up reaction. Therefore, the hardware trigger has a high probability to accept two uncorrelated events stemming from elastic scattering, which arrive within the coincidence window. This can be reduced and estimated exploiting the relative time-of-flight (TOF) between the two particles. The TOF is taken relative to the RF of the cyclotron. The left panel in Fig. 6.8 shows the TOF of the first particle plotted versus the TOF of the second particle. The prompt events are shown in the center of the pictures. The right panel in this figure shows the relative TOF, $(TOF2 - TOF1)$ where $TOF1$ and $TOF2$ are the TOFs of particles 1 and 2, respectively, with respect to the radio frequency of AGOR. It shows the difference between the arrival times of the two protons. Two particles with a relative TOF of less than 3 RF-cycles[1] could belong to a prompt break-up reaction. The gate shown in this figure indicates the selected prompt events.

The left panels in fig. 6.9 show the correlation between energy and TOF for one of the particles. The right panels show the corresponding correlation between the energies of the two protons. The effect of selecting different regions of the TOF spectra on the energy correlation between two protons is illustrated from the top to bottom panels in this figure. In this figure, the second row shows the effect of a cut on the prompt events within three RF-cycles in the relative TOF spectra. This gate contains all the "true" break-up events that arrived in the expected time gate of 130 ns. The remaining accidental background can be estimated from the accidental data outside the prompt TOF window. In the third

[1] Every RF-cycle lasts 16 ns

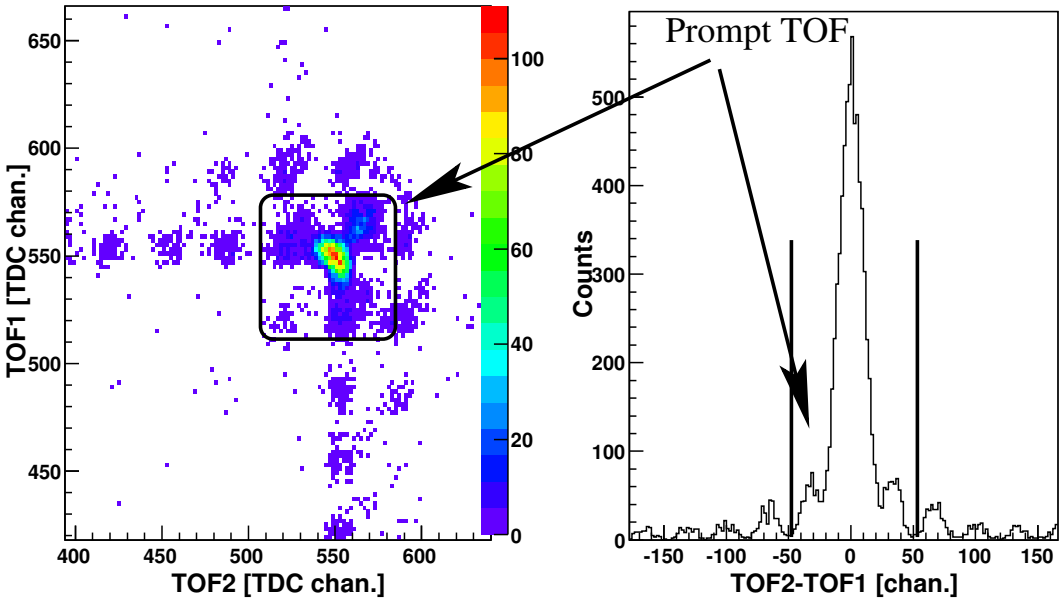

Figure 6.8: The left panel shows the TOF of the first particle plotted versus the TOF of the second particle. The prompt TOF events can be clearly seen in the center. The right panel shows the relative TOF, $(TOF2 - TOF1)$. The gate shown in this panel indicates the prompt events.

row, the effect of events at larger TOF values are shown. These events correspond to two uncorrelated protons from elastic scattering. The observed energy spectrum is distorted due to a mismatch in timing between the integration window of the QDC and the signal from the PMTs. At very large TOF values, only a small fraction of the PMT signal is integrated by the QDC, giving rise to a small energy response. The bottom row shows the effect of a cut on events at lower values of the TOF. Also, these events are accidental background from two elastic-scattering events. By using the events of the accidental background from the lower TOF region, the background within the prompt time window can be estimated and subtracted accordingly. A typical background of 2-20% for the kinematics with scattering angles (θ_1, θ_2) less than 20° and 2% for the kinemtics with (θ_1, θ_2) larger than 20° have been observed in the data analysis.

After subtracting the accidental background, we are left with true break-up events. Note that a significant amount of the remaining events lie below the expected S-curve. These events stem from protons of the break-up reaction which deposit less energy in the scintillators after undergoing a hadronic interaction. A large part of the energy escapes the detector via neutron emissions. The hadronic region is illustrated in Fig. 6.5. In the cross-section analysis, we only count events which deposit their full energy in the scintillator. The correction for the hadronic contribution is obtained from GEANT-3 simulations and is generally around 7-8% per particle for the energy range of 30-140 MeV.

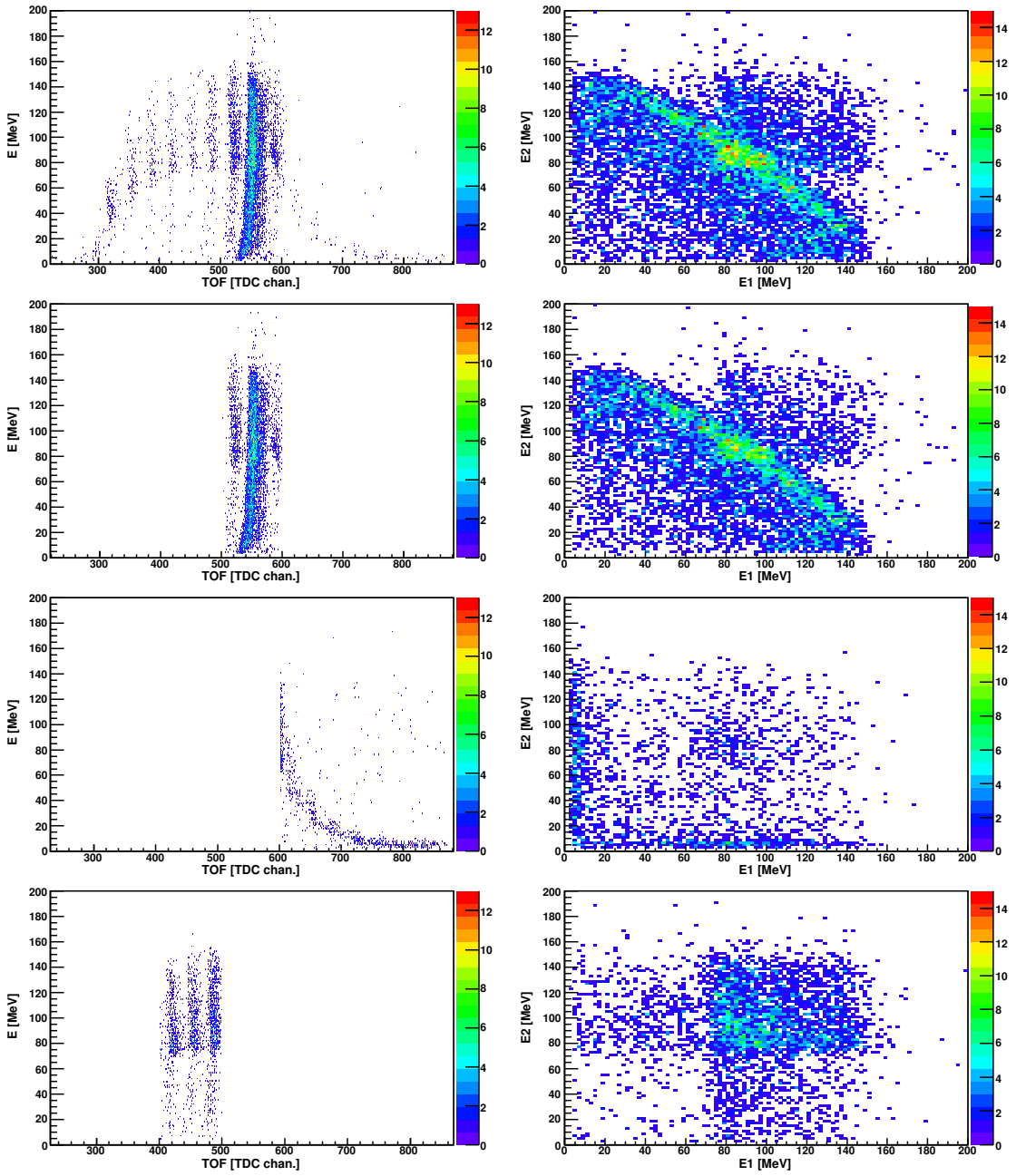

Figure 6.9: The effect of different TOF cuts on the energy correlation of two protons from the break-up reaction is shown. First column shows energy versus TOF for single particles, and second column shows the energy correlation between two particles. Second row shows the effect of prompt TOF cut, three RF-cycles. Third and forth rows show events with larger and smaller TOF values which include the accidental background of protons from two independent elastic-scattering events that make a coincidence. For more details, see text.

6.4 Energy projection on the S-curve

The number of break-up events in an interval $S-\Delta S$, and $S+\Delta S$ is obtained by projecting the events on a line perpendicular to the S-curve. The left panel in Fig. 6.10 shows the region that is projected on the perpendicular line to the S-curve. The projected spectrum is shown in the right panel of Fig. 6.10. This spectrum contains break-up events around channel 0 and background from accidental and hadronic events. We call this projection the D-axis. The zero point for the D-axis is defined by the crossing point with the S-curve.

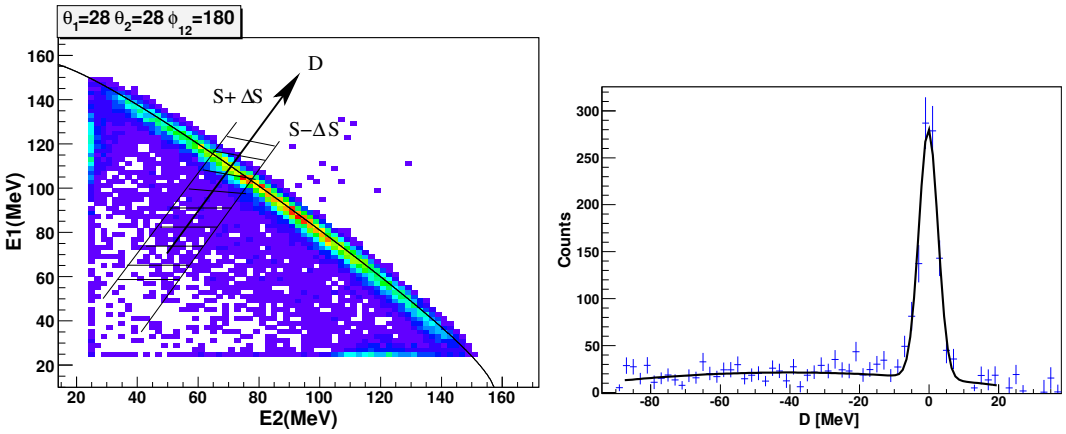

Figure 6.10: The energy correlation is shown between two protons in coincidence for the kinematical configuration, $(\theta_1, \theta_2, \phi_{12}) = (28°, 28°, 180°)$, together with the kinematical S-curve. The direction of the D-axis and the projection interval are also shown.

The accidental background is located at channels higher than the main peak in the left panel in Fig 6.11. This background can be subtracted using the TDC information, as explained earlier in this chapter. The result of this is shown in the right panel. In this case, the background level from time-uncorrelated events has been normalized to the background from the prompt events. The left panel in Fig. 6.11 shows the position of the background events in comparison to the true events for a typical kinematics and a typical value of S.

The hadronic background is located at the lower channels on the D-axis which corresponds to events below the S-curve in Fig. 6.10. As discussed before, these events are probably "true" break-up events. At this stage, this background is fitted together with the main peak around zero using a second-order polynomial (hadronic background plus a Gaussian signal). The right panel in Fig. 6.11 shows the result of the fit to the D-spectrum in the left panel after subtracting the random events. The number of events under the Gaussian peak will be referred to as the number of break-up events and will be used to obtain the cross section after efficiency corrections.

Since, in the background subtraction process, we removed the hadronic contribution from the break-up events, this contribution has to be added afterwords. The response of the detection setup to protons is obtained through a GEANT-3 (GEISHA model) simulation and is used to correct for the hadronic contribution. Figure 6.12 shows the GEANT simulation of the response of BINA for protons at $\theta = 25° \pm 1°$. The ratio of hadronic

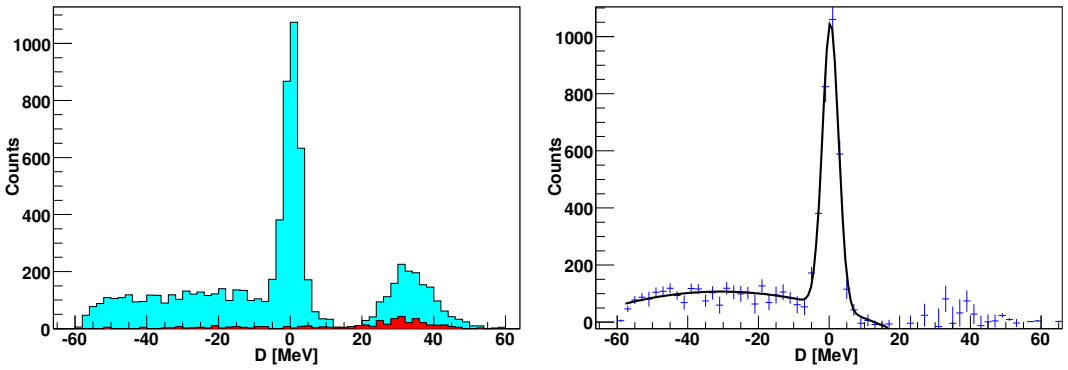

Figure 6.11: The left panel shows the D-curve for events within the prompt TOF gate as blue histogram. This histogram contains mainly the break-up events shown with light gray (cyan on-line) with a peak around channel 0, plus background from hadronic and the accidental events. Also, the shape of the background from elastic-scattering accidental events is shown as dark gray (red on-line) histogram. The right panel shows the blue spectrum after subtraction of the accidental background and fitting a second-order polynomial plus a Gaussian function. The quality of the fit is good with χ^2 ∼1.53.

events are extracted by normalizing the number of events outside the main peak to total counts. According to this simulation, ∼8% of the particles undergo a hadronic interaction in the scintillator material. This percentage fluctuates for different S-values by about $\sim$ 0.5%. The differences between the simulated and experimental shapes for suspected "hadronic" background is allocated to the systematic uncertainty.

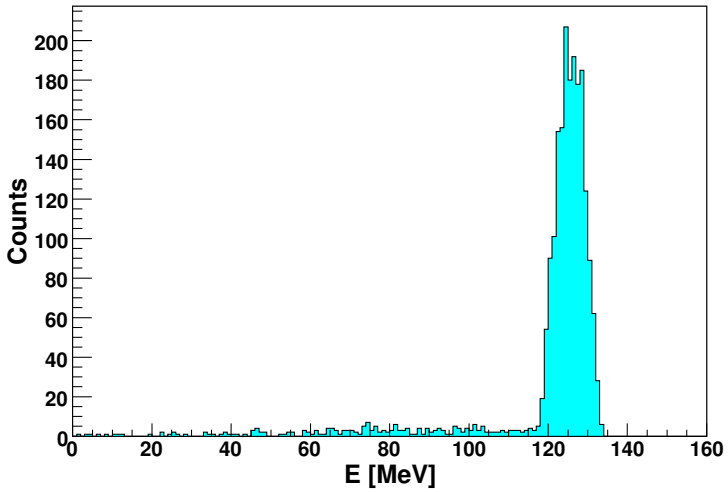

Figure 6.12: The deposited energy of protons of 125 MeV at $\theta = 25^\circ \pm 1^\circ$ in the scintillator material simulated by GEANT-3. The hadronic contribution is obtained by normalizing the number of events outside the main peak to the total number of counts.

6.5 The break-up cross section

The break-up cross section is presented for every configuration in which two protons are found in coincidence at fixed coordinates $(\theta_1, \theta_2, \phi_{12})$, within a small range $(\Delta\theta_1, \Delta\theta_2, \Delta\phi_{12})$. The cross section is obtained by counting the number of break-up events and is given as a function of S. The number of break-up events for every bin in S is obtained as follows:

1. The energy distribution between $S-\Delta S$, and $S+\Delta S$ is projected on a line perpendicular to the direction of S; see Fig 6.10.

2. The procedure for subtracting the background, explained in the previous section, is performed for: accidental events and hadronic events; see Fig. 6.11.

3. The number of events are corrected for the hadronic contribution, obtained by a GEANT-3 simulation.

In this section, we calculate the cross section directly by using the experimental parameters such as the beam current and the target thickness together with the different efficiencies of the system.

For a given kinematical configuration, $\xi(E_1, E_2, \theta_1, \theta_2, \phi_{12})$, the break-up cross section is defined as:

$$\frac{d^5\sigma}{d\Omega_1\, d\Omega_2\, dS} = \frac{N}{Q/Z} \cdot \frac{1}{t\cdot\epsilon} \cdot \frac{1}{\Delta\Omega_1\, \Delta\Omega_2\, \Delta S}, \tag{6.1}$$

where, N is the number of break-up events, Q, Z, t, and ϵ are introduced in Eq. 5.1, $\Delta\Omega_1, \Delta\Omega_2$ are the solid angles for the two protons, and ΔS is the size of the energy window placed on the S-curve. Figure 6.13 shows the cross section, $\frac{d^5\sigma}{d\Omega_1\, d\Omega_2\, dS}[\mu\mathrm{b/sr^2MeV}]$, as a function of S [MeV] for the coplanar kinematics, $(\theta_1, \theta_2, \phi_{12}) = (28^\circ, 20^\circ, 180^\circ)$. In this figure, the solid curve represents the Faddeev calculations using the CDB two-nucleon potential, the dashed line CDB+Δ, the dotted line CDB+Δ+Coulomb potentials from the Hannover-Lisbon theory group, and the dash-dotted line represents the CDB+relativistic potential from Bochum-Krakow group.

In this analysis, cross sections are determined by taking into account the following parameters and conditions:

1. The efficiency of MWPC for protons is applied for every $E-\Delta E$ hodoscope. The average efficiency of the MWPC for protons is ∼97% (see Chap. 5).

2. A correction factor of ∼8% per particle is applied for hadronic interactions as obtained by the GEANT-3 simulation.

3. The effective target thickness is 6.8 mm, including 0.8 mm due to bulging of the target.

4. The beam current and the live-time which were read out every second during the course of the experiment. The typical beam current is ∼10 pA, and the live-time is typically around 50%.

5. Events in which one of the two protons has an energy of less than 25 MeV were rejected.

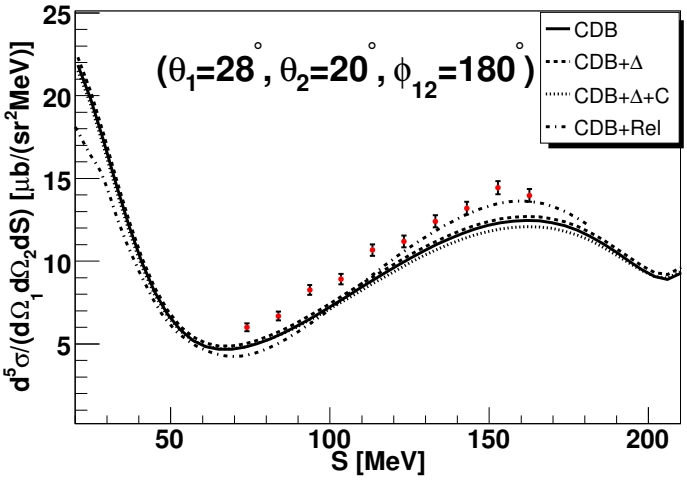

Figure 6.13: The cross section is plotted as a function of S [MeV] for the kinematical configuration, $(\theta_1, \theta_2, \phi_{12}) = (28°, 20°, 180°)$. Lines represent Faddeev calculations from the Hannover-Lisbon, and Bochum-Krakow groups. The solid line represents the cross section using CDB two-nucleon potential, the dashed line shows results of the calculations, CDB+Δ, which includes the effects of the three nucleon force, the dotted line is the CDB+Δ+Coulomb, and dash-dotted line represents CDB+relativistic calculations.

6. Events with a prompt TOF window within 3 RF-cycles were selected.

Since the threshold in this experiment was set to ∼25 MeV in order to cut the events that punch through the scintillators, we do not measure cross sections for the complete range in S. This lower threshold cuts the tails of the cross section at higher and lower S. For the configurations for which the accidental background events overlap with break-up events, the background subtraction procedure does not work successfully for all cases. The corresponding data were, therefore, not analyzed.

The stability of the measured cross section as a function of time was checked by using one of the kinematics that has a high cross section, e.g. the configuration $(\theta_1, \theta_2, \phi_{12}) = (28°, 28°, 180°)$. The data are divided into smaller time steps of 1 hour each and the cross section for every value of S and for every time slice is extracted. Figure 6.14 shows the measured cross sections as a function of time (run No.). The average value of the cross section for each S-value is calculated by fitting a constant line to the data. The low reduced χ^2 value of the fit ~ 1 for every S-bin shows that the fluctuations behave statistically.

6.6 The scattering asymmetry and the analyzing power

The interaction of a polarized beam with an unpolarized target produces an azimuthal asymmetry in the scattering cross section. The magnitude of this asymmetry is proportional to the polarization of the beam and an observable that is called the analyzing power. The procedure of obtaining the analyzing power in the break-up channel is similar to that for the elastic channel. For every kinematical point, ξ, the azimuthal distribution of the scattered particles for polarized beam is normalized to that of the unpolarized beam. The

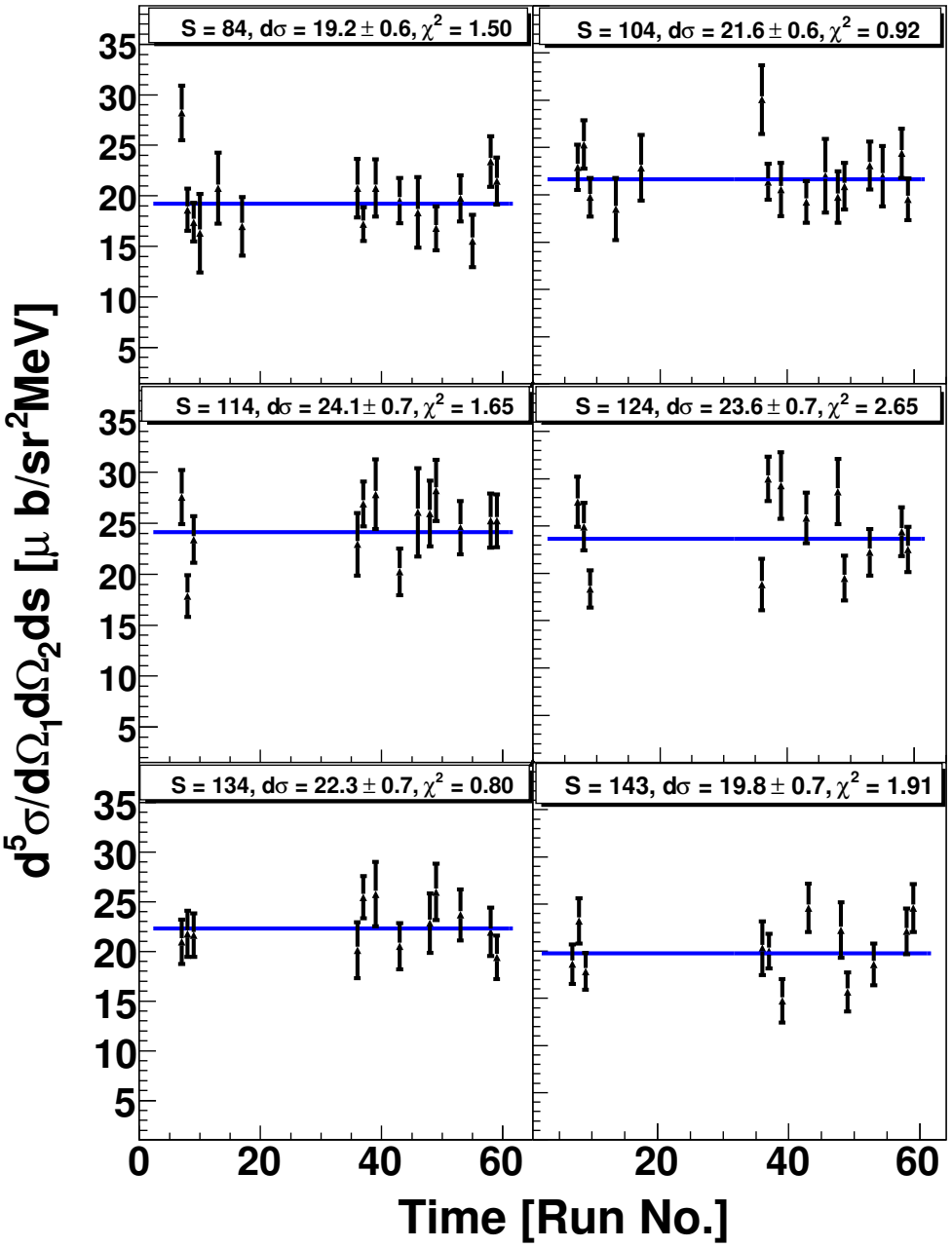

Figure 6.14: Results of the cross section for many S-values (in MeV) in the coplanar configuration, $(\theta_1, \theta_2, \phi_{12}) = (28°, 28°, 180°)$, as a function of time. The average value of the cross section for each S-value is calculated by fitting a constant line to data as a function of time.

analyzing power of the break-up reaction is presented in a similar way as was done for the

analyzing power in the elastic reaction, namely:

$$\sigma(\xi) = \sigma_0(\xi)(1 + A_y(\xi)\, p_Z\, \cos\phi), \tag{6.2}$$

where σ, σ_0 are the polarized and unpolarized cross sections, respectively, ξ is explained in Chap. 2, A_y, p_Z are the vector-analyzing power and the beam polarization, respectively, and ϕ is the azimuthal scattering angle of one of the outgoing protons.

Using Eq. 6.2, the reaction asymmetry, $A_y \cos\phi = \frac{\sigma^{\downarrow} - \sigma^{\uparrow}}{\sigma^{\uparrow} p_Z^{\downarrow} - \sigma^{\downarrow} p_Z^{\uparrow}}$, is calculated by exploiting the distribution of events obtained with beam with polarizations up ($\uparrow$) and down ($\downarrow$) and the value of beam polarization in these two modes. This gives a periodic function in ϕ and the amplitude of the periodic function corresponds to A_y. The beam-polarizations, $p_Z^{\uparrow,\downarrow}$, are determined from the analysis of the elastic channel. Figure 6.15 shows the asymmetry as a function of ϕ for a particular bin in S.

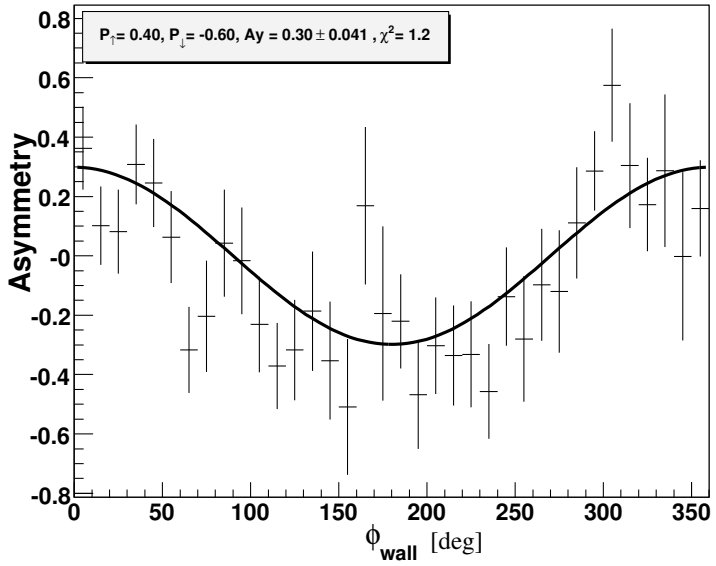

Figure 6.15: The asymmetry in the break-up reaction, $\frac{\sigma^{\downarrow} - \sigma^{\uparrow}}{\sigma^{\uparrow} p_Z^{\downarrow} - \sigma^{\downarrow} p_Z^{\uparrow}}$, as a function of the azimuthal scattering angle of one of the protons, ϕ_{wall}. The curve represents a function of the form $A + B\cos\phi$, where $A \simeq 0$ is an offset and $B = A_y(\xi)$.

By exploiting the asymmetry distribution for each S-bin, the vector-analyzing power, A_y, is obtained for every kinematical configuration, $(\theta_1, \theta_2, \phi_{12})$. Figure 6.16 shows an example of an analyzing-power measurement for $(\theta_1, \theta_2, \phi_{12}) = (28°, 25°, 180°)$. The various lines represent calculations from the Hannover-Lisbon and Bochum-Krakow theory groups which were explained in the caption of Fig. 6.13.

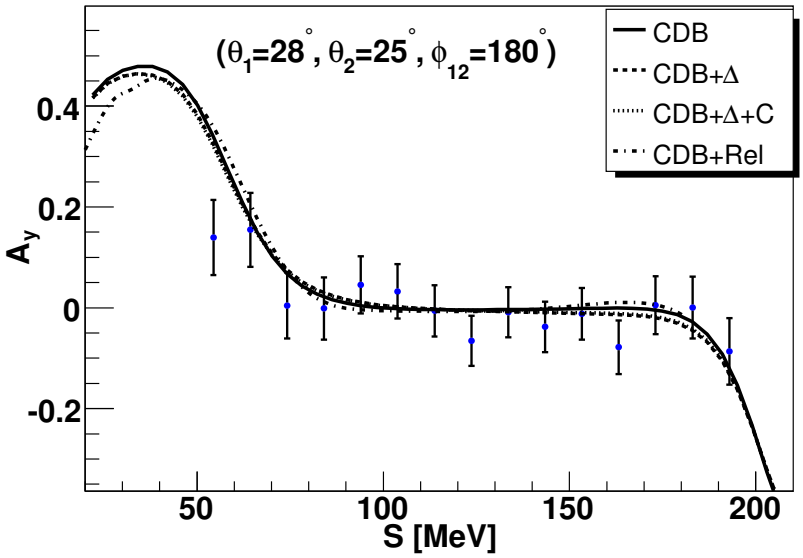

Figure 6.16: The result of an analyzing-power measurement for the coplanar kinematics, $(\theta_1, \theta_2, \phi_{12}) = (28°, 25°, 180°)$, as a function of S. For a description of the curves, see the caption of Fig. 6.13.